AIAA JOURNAL
Vol. 45, No. 6, June 2007

# Adaptive Closed-Loop Separation Control on a High-Lift Configuration Using Extremum Seeking

Ralf Becker* and Rudibert King†
*Berlin University of Technology, 10623 Berlin, Germany*
and
Ralf Petz‡ and Wolfgang Nitsche§
*Berlin University of Technology, 10587 Berlin, Germany*

DOI: 10.2514/1.24941

**We present experimental results on adaptive closed-loop separation control on a 2-D generic high-lift configuration. Because model-based closed-loop flow control suffers from the lack of sufficient simple physical models for this configuration, a non-model-based control strategy, namely, the gradient-based extremum-seeking scheme, is used here. The controller exploits spanwise distributed pressure measurements and adjusts pulsed jets near the leading edge of the single-slotted flap. The jets are used for flow excitation to suppress separation over the flap at high angles of attack, high deflection angles, or to reattach an already separated flow. Starting from a single-input/single-output design, the extremum-seeking scheme is extended to both a single-input/single-output slope-seeking approach and a multi-input/multi-output approach. Multi-input/multi-output control accounts for spanwise-distributed, small-scale separation phenomena and shows the best performance. Additionally, this case even improves lift gain compared to preliminary open-loop studies. A lift increase is not only observed for angles of attack for which the unactuated flow obviously separates, but as well for smaller angles, which were assumed before to lead to an unseparated flow. Hence, closed-loop results demonstrate the capability of slope-seeking control to adjust the control signal automatically in an energy-efficient sense such that separation is minimized even in the presence of disturbances.**

## Nomenclature

| | | |
|---|---|---|
| $A$ | = | main wing area $lc_{\text{main}}$ |
| $a$ | = | amplitude of harmonic perturbation |
| $c_D$ | = | drag coefficient $D/(A\frac{\rho}{2}U_\infty^2)$ |
| $c_L$ | = | lift coefficient $L/(A\frac{\rho}{2}U_\infty^2)$ |
| $c_{\text{main}}$ | = | chord length of main airfoil |
| $c_p$ | = | pressure coefficient, $(p-p_\infty)/(\frac{\rho}{2}U_\infty^2)$ |
| $c_R$ | = | nondimensional roll moment $M/(A\frac{\rho}{2}U_\infty^2\frac{l}{2})$ |
| $c_\mu$ | = | nondimensional excitation momentum coefficient $2\frac{h}{c_{\text{main}}}(\frac{U'}{U_\infty})^2$ |
| $D$ | = | drag force |
| $f(u)$ | = | steady-state input–output map |
| $f'_{\text{ref}}$ | = | reference/commanded slope of $f$ |
| $G_{\text{HP}}(s)$, $G_{\text{LP}}(s)$ | = | high-pass and low-pass filter transfer functions |
| $L$ | = | lift force |
| $l$ | = | wing span |
| $l_a$ | = | chord length from actuator position to flap trailing edge |
| $M$ | = | roll moment |
| $p$ | = | pressure |
| $Re_c$ | = | Reynolds number based on chord length |
| $St$ | = | Strouhal number of pulse excitation $\frac{fl_a}{U_\infty}$ |
| $t$ | = | time |
| $U$ | = | velocity |
| $U_\infty$ | = | freestream velocity |
| $U'$ | = | phase-locked rms amplitude of the velocity close to the excitation slot (still air) |
| $u$ | = | control input |
| $u_0$ | = | initial value of $u$ |
| $u^*$ | = | optimal/desired $u$ |
| $\hat{u}$ | = | estimate of $u^*$ |
| $y$ | = | steady-state system output |
| $y_0$ | = | initial value of $y$ |
| $y^*$ | = | maximal/desired $y$ |
| $\alpha$ | = | angle of attack |
| $\delta_f$ | = | flap deflection angle |
| $\omega$ | = | angular frequency of harmonic perturbation |
| $\omega_{\text{HP}}$, $\omega_{\text{LP}}$ | = | high-pass and low-pass filter cutoff frequencies |

Presented at the 3rd AIAA Flow Control Conference, San Francisco, 5–8 June 2006; received 3 May 2006; revision received 23 January 2007; accepted for publication 24 January 2007. 

*Research Engineer, Measurement and Control Group, Department of Process and Plant Technology, Hardenbergstrasse 36a.

†Professor and Corresponding Author, Measurement and Control Group, Department of Process and Plant Technology, Hardenbergstrasse 36a; Rudibert.King@tu-berlin.de.

‡Research Engineer, Aerodynamics Group, Department of Aeronautics and Astronautics, Marchstrasse 12.

§Professor, Aerodynamics Group, Department of Aeronautics and Astronautics, Marchstrasse 12.

## I. Introduction

EXPLOITING flow instabilities, active flow control (AFC) can significantly enhance the region of operation compared to passive means, such as riblets or vortex generators. Moreover, for increased flexibility the actuation may be optimally adapted over a wide range of operating conditions simultaneously, rejecting disturbances and avoiding the negative effects of passive flow control in situations where no flow control is needed. Typical examples of actuation in AFC include suction and blowing, acoustic actuation, or synthetic jets. Active flow control technology can reduce drag and noise, or can increase the lift of airfoils. Literature surveys, including actuation mechanisms and sensor applications, are given in Fiedler and Fernholz [1], Gad-el-Hak et al. [2], and Gad-el-Hak and Bushnell [3]. A detailed study concerning the potential benefits of applying unsteady separation control to civil transport aircraft is given in McLean et al. [4].

The present investigation focuses on high-lift systems, which have to provide very high lift coefficients in low-speed flight during takeoff or landing. At high angles of attack, the flow over high-lift wings may separate, resulting in a reduction of lift and increase in drag. Thus, active separation control has become an increasingly attractive topic in the last few years (see, for example, Pack et al. [5,6]). If the onset of separation could be delayed towards higher angles of attack, it will either be possible to achieve a higher lift for steeper landing and climbing paths, or to reduce mechanical complexity of high-lift systems.

Application of active control, however, necessitates a self-sustaining, autonomously working control system. Such control systems have to face the problem of uncertainties, for example, uncertain flow conditions that may result in uncertain system behavior, or external disturbances if the control system is used in a real environment outside the well-defined conditions of a laboratory wind tunnel. In contrast to open-loop control, which has demonstrable benefits in environments with well-defined conditions, closed-loop control can drive the actuation mechanism such that uncertain system behaviors and/or disturbances are compensated for as well. Hence, only by closed-loop control can the flexibility and robustness that are needed in real, disturbed environments be guaranteed. However, the requirement of a real-time capability for calculating the control law, including A/D and D/A conversions, preprocessing of sensor readings, etc., means that many classical closed-loop controller synthesis methods, which are based on a mathematical model of the flow process, are not suited for the inherently nonlinear fluid flow systems that are of interest.

Although, recently, various attempts have been made to use closed-loop separation control, most of the work published so far is dedicated to open-loop control. Furthermore, experimental validations of closed-loop flow control are still rather rare. The use of low-dimensional models for controller synthesis, which are directly based on the Navier–Stokes equation, that is, Galerkin and vortex models, is still restricted to rather simple flow configurations (see, for example, King et al. [7]), and need a rather detailed knowledge of the system.

Recent experimental results are presented by Caraballo et al. [8], Glauser et al. [9], and Siegel et al. [10]. Allan et al. [11], King et al. [12], Becker et al. [13–15], Garwon and King [16], and Henning and King [17] propose the use of low-dimensional black-box models for robust and adaptive controller synthesis for control of high-lift configurations, the backward-facing step, a diffusor, turbomachines, and a bluff body. Moreover, model-free approaches, such as extremum-seeking control for updating different excitation signal parameters have been exploited in experimental studies by Banaszuk and Narayanan [18], Garwon et al. [19], Garwon and King [16], Henning and King [17], and Beaudoin et al. [20]. This model-free approach will be used here as well for the 3-D control of a high-lift configuration.

Preliminary wind-tunnel experiments, see Petz et al. [21], revealed that the strong nonlinear dynamics of our high-lift test configuration includes saturation and hysteresis effects that lead to significant detuning of the aforementioned black-box model-based controllers. Thus, the present investigation explores extremum-seeking control as a possible, non-model-based alternative for closed-loop separation control. Three different control designs are implemented in wind-tunnel experiments and compared. The excitation technique is described in more detail in Petz and Nitsche [22].

The paper is organized as follows: A description of the configuration is given in Sec. II. Sections III and IV describe the extremum-seeking control schemes and experimental results, respectively. Finally, the results are summarized.

## II. Experimental Setup and Temporal Averaged Characteristics

### A. Wind-Tunnel Model

All experiments are performed in a closed-loop wind tunnel with a low level of turbulence of 0.3%. The high-lift test configuration is placed inside the test section (2000 × 1400 mm). A six-component wind-tunnel balance is placed underneath the test section to measure the difference between base flow and excited flow in terms of lift, drag, and roll moment. The freestream velocity is adjustable from 0 to 30 m/s, resulting in a maximum chord Reynolds number $Re_c = 10^6$. All results presented here are obtained at Reynolds numbers around $0.5 \times 10^6$ corresponding to $U_\infty = 15$ m/s, but tests with higher Reynolds numbers up to $1 \times 10^6$ were conducted as well. Further details about the experimental setup can be found in Petz and Nitsche [22] and Petz et al. [21].

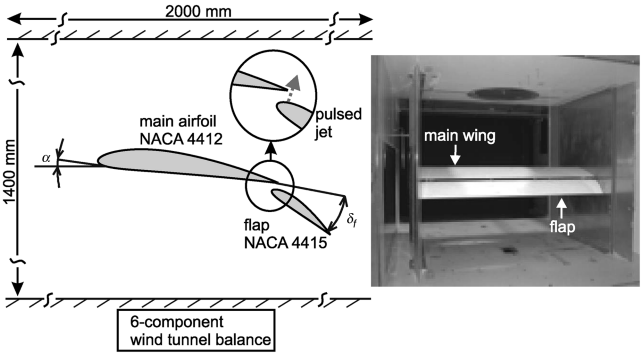


**Fig. 1 Left: sketch of the wind-tunnel model; right: rear view of the model in the test section.**

The generic two-element high-lift configuration consists of a main wing with a single-slotted trailing-edge flap. Both main wing and flap have a NACA-type airfoil shape as shown in Fig. 1. The flap has a chord length of $0.4c_{\text{main}}$, with $c_{\text{main}} = 500$ mm, and is fixed relative to the main wing, with a flap gap of $3.5\%c_{\text{main}}$, and a flap overlap of $2.7\%c_{\text{main}}$. The angle of attack $\alpha$ and flap deflection angle $\delta_f$ are individually adjustable. The geometric configuration of the wing and the flap is completely 2-D with the exception of four flap tracks; see Sec. IV.D. Both main wing and flap are equipped with trip wires at the leading edges to fix the transition and guarantee turbulent separation.

Flow is excited by a pulsating wall normal jet. Figure 2 shows a simplified sketch of the actuator arrangement inside the flap. The pulsed jet blows through a spanwise continuous thin slot that is located at the flap upper surface at $x/c_{\text{flap}} = 0.035$. A thin slot (slot width = 0.3 mm), covering 81% of the total flap span, is fabricated into the flap surface. The size of the model, wing span of 1550 mm, allows the actuator to be placed inside the flap. To achieve a homogeneous jet velocity distribution in spanwise direction, the actuator is subdivided into 11 actuator segments. Each segment consists of a small, fast switching solenoid valve connected to a specially designed plenum that distributes the air to the complete actuation segment span of 114 mm. The pulses used for flow excitation are generated by the solenoid valves, which only have the two states, open and closed. The amplitude of the excitation is continuously adjustable through a pressure regulator valve that simultaneously controls the pressure of all 11 actuator segments. A fast programmable microcontroller is used to adjust the forcing frequency and to manage the open and close times of the solenoid valves, the so-called duty cycle. The excitation mechanism is designed to produce amplitudes in the range of the freestream velocity ($U_{\text{jet}}/U_\infty = 1$). The complete actuator is calibrated using a

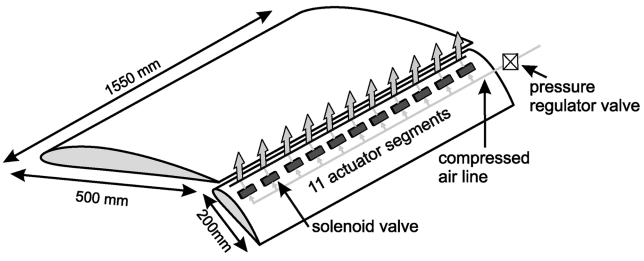


**Fig. 2 Sketch of the wind-tunnel model and actuator assembly with 11 spanwise distributed segments.**

single traversable hot wire and fast pressure transducers attached to the 11 segments.

### B. Experimental Uncertainties

The experimental uncertainty in the determination of forces and moments using the balance system was estimated to be 0.1% for lift, drag, side force, and yaw moment, and 0.3% for the rolling and pitching moment. The gap between the model and the side walls was narrowed to 0.1 mm to minimize leakage effects and pressure equalization from the upper to the lower wing surface. However, the error cannot be quantified because no exact data are available for comparison. The obtained forces and moments are corrected using a standard 2-D wind-tunnel wall correction method [23].

The pressure sensor used for sensing the pressure distribution on the main wing has an accuracy of 0.5%. The transducers used for the excitation system and the pressure distribution on the flap have a resolution of less then 0.5 Pa and are able to measure pressure fluctuations up to 1 kHz. Because of the installation of the transducers that are connected to short pressure lines, the cutoff frequency is reduced to 0.5 kHz (experimentally determined).

The angle of attack is adjusted by a stepper motor with a gear transmission ratio of 820:1. The repeatability lies well within 0.1 deg. The flap deflection angle is adjusted by two stepper motors placed inside the main wing, each having a transmission ratio of 40:1. The rotating motion is transferred to the flap via a V-ribbed belt. To account for the angle uncertainty, a tilt sensor is installed inside the flap, which has a resolution of 0.1%. The actuator is calibrated in still air using a traversable hot wire. The hot wire is placed as close to the excitation slot as possible to measure the correct jet velocity. This is a crucial part for the calculation of the nondimensional momentum coefficient. The complete frequency and amplitude ranges are measured to calculate the corresponding $c_\mu$. Because of the length of the actuator slot of 1254 mm, the calibration was carried out only at discrete locations of each actuator segment. The cited $c_\mu$ values are therefore within $\pm 15\%$ of the actual values.

### C. Online Measurements

To close the control loop in the experiments, preliminary tests were undertaken to figure out a reliable and easy way to detect flow separation on the flap [21,22]. Measurements of static streamwise pressure differences on the flap proved to be the easiest way. For that purpose, the wind-tunnel model flap was instrumented with 22 additional pressure orifices downstream of the excitation slot. Two orifices were placed in the midsection of each actuation segment to measure the pressure difference $\Delta c_p$, which gives a good and fast indication about the attached/separated flow state with respect to the closed-loop bandwidth. The separated case yields a $\Delta c_p$ around zero, whereas in the fully attached flow $\Delta c_p$ is clearly above 1. The change of pressure difference is monitored by fast transducers to minimize the reaction time for the controller. A series of tests examining the onset and end of flow separation on the flap showed that there is agreement between the measured pressure differences and the lift measurements from the balance system.

### D. Time-Averaged Characteristics

It has been demonstrated in a number of experiments that periodic flow excitation results in a significant increase in lift [24]. This section briefly illustrates the benefits of local periodic forcing in terms of increased lift, drag reduction, and a predictable roll moment in an open-loop control mode.

The effectiveness of excitation for active control of flow separation depends on several parameters. First, the location of the excitation is a dominant factor. Second, the forcing frequency and excitation amplitude have to be correctly prescribed to affect the separated flow sufficiently. The remaining parameters, such as duty cycle of the solenoid valves, number of active actuator segments, angle of attack, or flap deflection, to name just a few, increase the complexity of the active flow control system. To reduce the number of governing parameters for the investigation in the temporal averaged characteristics, forcing frequency, and amplitude of the pulsed air excitation are set to fixed values obtained in preliminary tests. The most successful frequency in terms lift enhancement for different excitation amplitudes is found at around 70 Hz, giving a Strouhal number of $St = 0.9$. The pulse duty cycle is set to 0.5, which means that the solenoid valves are half-period open and half-period closed.

Figure 3 illustrates the benefits of periodic excitation for two different examples. The plot on the left displays lift coefficient $c_L$ plotted against angle of attack $\alpha$. These data measured by the balance system are corrected using a standard wind-tunnel wall correction method [23]. Flap deflection is set to a fixed value of $\delta_f = 32$ deg. The unexcited case shows a significant lift drop at around $\alpha = 2$ deg resulting from a separation on the flap. The lift then increases linearly with increasing $\alpha$ until the flow separates on the main wing ($\alpha = 7$ deg). Maximum lift is increased by up to 12%. A positive effect is also seen in the drag reduction due to the elimination of the separation region. As a result, the lift-to-drag ratio, describing the aerodynamic quality, is improved in this case by a maximum of 22%.

The plot on the right side of Fig. 3 shows the effect of local (distributed) spanwise excitation. This is possible due to the

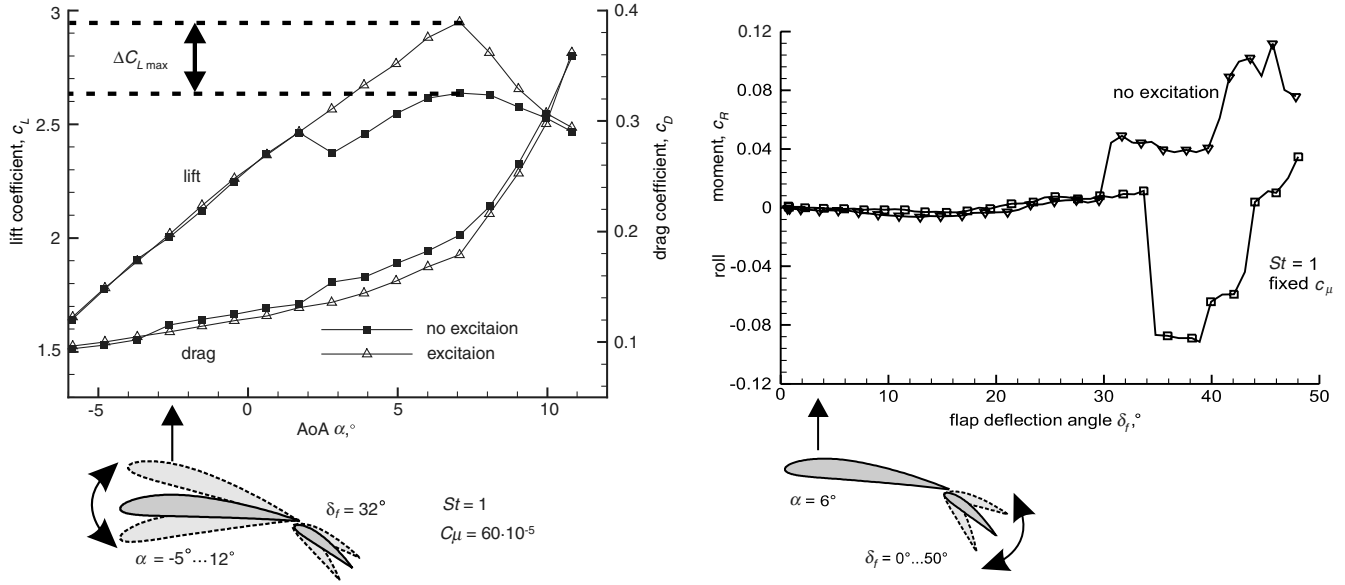


**Fig. 3 Left: lift vs angle of attack with and without active flow control; right: roll moment generated by local spanwise excitation.**

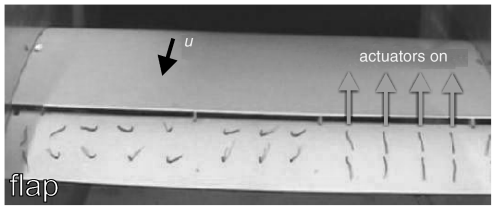


**Fig. 4 Rear view of the test model with wool tufts on the flap.**

spanwise segmentation of the actuator setup and the ability to individually control each segment. In the presented case, only four actuator segments on the right side of the flap are used to locally attach the flow and thus generate a roll moment. Without control, the roll moment is slightly positive and is to some extent unpredictable due to the unsteady behavior of the large separation region. Separation is delayed by a few degrees using local spanwise excitation. A strong negative roll moment is generated due to the attached flow on the right side. Figure 4 shows a view of the aft portion of the model with wool tufts placed on the upper side of the flap; the attached flow over the right side of the flap and the separated region on the left can be seen.

## III. Real-Time Optimization by Extremum-Seeking Control

If active flow control is to be applied in the future, a closed-loop control system is required to account for disturbances arising from an incomplete knowledge of the flowfield and uncertainties in the system description. An autonomously working sensor–controller–actuator system that uses sensor readings to detect the flow condition (attached or separated), a robust controller to calculate appropriate control signals, and well-designed actuators to modify the flow must be developed [11]. This basic principle is applied to the high-lift configuration in the following, and three different control strategies are tested.

Preliminary studies showed that extremum-seeking control is the most effective and most practical control method for the high-lift application. This method has been used in other studies for flow control applications [12,25,26]. The basic extremum-seeking scheme is next described, and then its generalized formulation for slope-seeking is reviewed.

### A. SISO Design

Extremum-seeking control is an appropriate, non-model-based method for the control of nonlinear plants that are characterized by an output extremum in the steady state [26,27]. The plant is considered as a block with the input $u$, that is, the control input, and the output $y$ to be controlled, with a static input–output map $y = f(u)$. Figure 5 shows the structure of the basic single-input/single-output (SISO) extremum-seeking control scheme for maximization. The idea is to perform a gradient-based online optimization to adjust the control input to $u^*$ such that the maximal steady-state system output $y^*$ is achieved without knowing the steady-state input–output map $y = f(u)$ and especially its extremum $y^* = \max y = f(u^*)$; see the right side of Fig. 5.

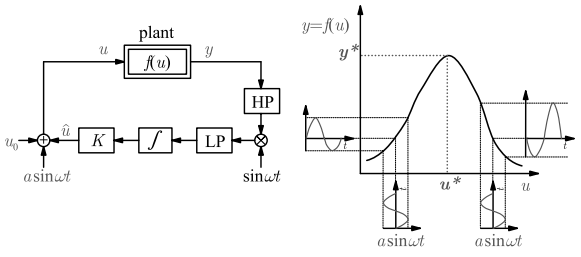


**Fig. 5 Block diagram of the basic extremum-seeking feedback scheme for maximization.**

The initial control input $u_0$ is calculated by some higher level control hierarchy or set to zero, see Fig. 5, and is superimposed with a sine signal $a \sin \omega t$, which has a small amplitude $a$. If the period of the harmonic perturbation is larger than the largest time constant of the dynamic plant, an approximate sinusoidal output $y$ will be obtained, initially around $y_0 = f(u_0)$. This output perturbation is analyzed to detect the slope (gradient) of the input–output map and then used for gradient-based optimization. To do so, the system output is passed through a high-pass filter (HP), which removes the mean value, initially $y_0$, but not the sinusoidal perturbation with frequency $\omega$. The product of this filtered output and the zero-mean sine signal $\sin \omega t$ gives a measure of the slope. This product leads to a non-zero-mean signal as long as the maximum is not obtained. If the plant is initially to the left of the maximum, the input and output perturbations are in phase, that is, the product will be positive. On the other hand, an antiphase relation that gives a negative product is an indication that the plant is to the right of the maximum. This product is then passed through a low-pass filter (LP) to extract a mean value. An additional term $\hat{u}$, added to $u_0 + a \sin \omega t$, is then calculated by time integration of this mean value and multiplication by $K$. As long as the output of the LP is positive, that is, the system is on the left side of the maximum, an increasing value $\hat{u}$ is obtained. For a negative output of the LP, the opposite is true. A minimum is obtained accordingly with this method.

The extremum-seeking scheme is an adaptive closed-loop type of control and guarantees closed-loop stability if designed properly; see Krstic and Wang [27] and Ariyur and Krstic [26] for details. The choice of certain design parameters determines the speed of convergence. The cutoff frequencies of the HP and the LP need to be lower than the frequency $\omega$ of the perturbation signal. In addition, the adaption gain $K$ needs to be small. Thus, the overall feedback system has fast, medium, and slow time scales corresponding to the plant dynamics, the periodic perturbation, and the filters in the extremum-seeking scheme, respectively. If the plant behavior varies due to uncertainties, the time scales of the perturbation signal and the filters have to be larger than the slowest possible plant dynamics. The main advantage of this extremum-seeking control is that no plant model is needed for controller synthesis. A penalty, however, is that permanent input and output perturbations arise, which are harmonic. Moreover, due to the slowly changing perturbations, the closed-loop control bandwidth is low.

### B. Slope Seeking as a Generalized Design

Slope seeking is an extension of the extremum-seeking scheme; for details see Ariyur and Krstic [26]. It involves driving the plant output to a value that corresponds to a commanded or reference slope of the steady-state input–output map, $y = f(u)$. Therefore, the negative value of the commanded slope $f'_{\text{ref}}$ is added to the actually detected slope; see Fig. 6. By this, the apparent extremum is shifted. Because extremum seeking is a special case of slope seeking, when the reference slope is zero, designing the filters, the integrator gain, and the sinusoidal perturbation are the same.

### C. Implementation

In this work, the controllers are tuned in experiments. In a first experiment, the pulsed excitation is switched on and off to estimate the transient time of the output variable to be controlled, that is, the pressure recovery. Based on this estimated system dynamics, the

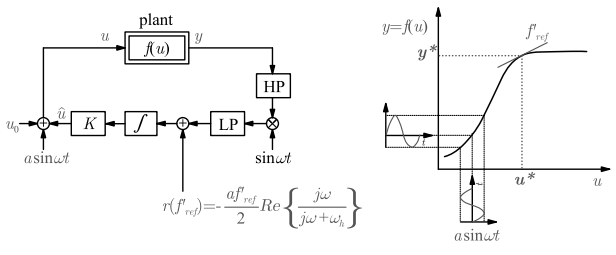


**Fig. 6 Block diagram of the basic slope-seeking feedback scheme.**

frequency of the sinusoidal perturbation signal was chosen such that its period is well separated from the transient time. The period of the perturbation signal with frequency $\omega$ is chosen to be seven times longer than the longest estimated transient time, giving $\omega = 1.4$ rad/s for the present setup. Based on this, the cutoff frequencies $\omega_{HP}$ and $\omega_{LP}$ of the HP and LP filters are five times lower than the perturbation frequency $\omega$ to guarantee a negligible phase shift at frequency $\omega$. Here, simple linear filters $G_{HP}(s) = s/(s + \omega_{HP})$ and $G_{LP}(s) = \omega_{LP}/(s + \omega_{LP})$ are implemented.

The integration time scale has to be well separated from the perturbation signal by using an appropriate low integration gain $K$ (see Figs. 5 and 6). Here, the gain is set to $K = 11$.

If the output perturbation is contaminated by noise, the noise has to be averaged out by an appropriate lower choice of the cutoff frequency $\omega_{LP}$ of the LP. This would lead to a slower adaption time scale corresponding to a lower control bandwidth. To avoid such detuning, the amplitude of the input perturbation is chosen high enough so that the output perturbation noise can be neglected.

## IV. Separation Control by Extremum-Seeking Control

Because a 2-D high-lift test model is used in the present investigation, a simple SISO type of extremum-seeking control for separation minimization is first implemented and tested; see Sec. IV. B. However, the results obtained show that after a change of the flow conditions to a situation in which no excitation is needed, this design is not able to decrease actuation automatically again. Thus, the extremum-seeking design is extended to SISO slope seeking; see Sec. IV.C. Despite the simplicity of the 2-D test model, a spanwise nonuniform flow structure occurs. Thus a multi-input/multi-output (MIMO) slope-seeking control, which significantly improves the performance, is also examined; see Sec. IV.D. However, before these control applications are described, possible plant input signals are discussed in Sec. IV.A.

### A. Possible Control Inputs from an Experimental Point of View

Because there are many adjustable parameters to be controlled in this kind of experiment, the best way to optimize the system would be a closed-loop system with as many different controller outputs, that is, plant inputs, as possible. In our experiments it would have been very useful to optimize excitation frequency, amplitude, and duty cycle simultaneously. Closed-loop strategies with all three parameters were tested. From a flow physics point of view, the frequency optimization would be very helpful because the frequency would be constantly varied and adapted to different flap deflections. However, because the sensitivity of the degree of separation with respect to the frequency was very weak in the range of operation of our actuators, the frequency was fixed for most of the experiments. Moreover, besides hardware requirements from the real-time controller, the experimental setup did not allow for a simultaneous adaption of the amplitude and duty cycle in the MIMO case; see Sec. IV.D. Therefore, only the results of the amplitude or duty cycle variations are presented in this paper.

Ruling out the frequency, the excitation amplitude is probably the best controller output signal because one can save a lot of energy by letting the controller find an optimum. Unfortunately, only a SISO approach (see Secs. IV.B and IV.C) could be realized in our experiments because all actuator segments share a common pressure supply that is controlled by two flow control valves. Moreover, during preliminary tests it turned out that the controller was not fast enough to react to sudden changes in flow conditions, for example, flap deflection settings. The reaction time of the flow control valves increased the dead time of the system to be controlled, and, hence, made it very difficult to adjust the controller parameters.

After ruling out frequency (for all designs) and amplitude (for the MIMO setups) the duty cycle is the only parameter left with a very short reaction time and the ability to control each actuator segment individually (see Sec. IV.D). Furthermore, by controlling the duty cycle it is possible to close the valves and save energy in the case of locally attached flow. Hence, the duty cycle, being the only controller output variable presented in this paper in the MIMO case, represents a compromise only. The excitation amplitude controlled by the supply pressure was set to the maximum pressure available ($4 \times 10^5$ Pa) in this case.

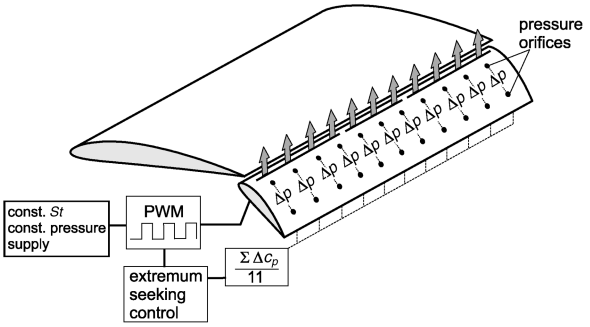


**Fig. 7 Sketch of the SISO control setup with excitation amplitude as control signal and spanwise-averaged pressure difference as output signal to be controlled.**

### B. Separation Control by SISO Extremum Seeking

#### 1. SISO Extremum Seeking Setup

SISO extremum-seeking control, see Fig. 5, with only one online measurement and one control input, is the most simple setup. Here, the excitation used for the preliminary open-loop experiments, see Sec. II.D, is extended by an extremum-seeking controller. Figure 7 shows the SISO setup. The spanwise-averaged pressure difference, that is, the flow system output to be controlled, is evaluated by the control scheme to compute the control input $u$, that is, the input voltage of the pressure regulator valve of the air supply, such that the averaged pressure difference is maximized. This control input yields a spanwise uniform amplitude of the air pulse excitation that is realized through the pulse width modulation (PWM) of the power supply; see Fig. 7. Because the other excitation parameters, that is, actuation frequency and duty cycle (set to 0.5), are fixed as in the preliminary open-loop investigations, the amplitude of the actuation is the only variable used to adjust the effectiveness of the separation control.

#### 2. Results

For varying flap deflection angle $\delta_f$ and fixed angle of attack $\alpha = 7$ deg, a comparison of force balance measurement results of a

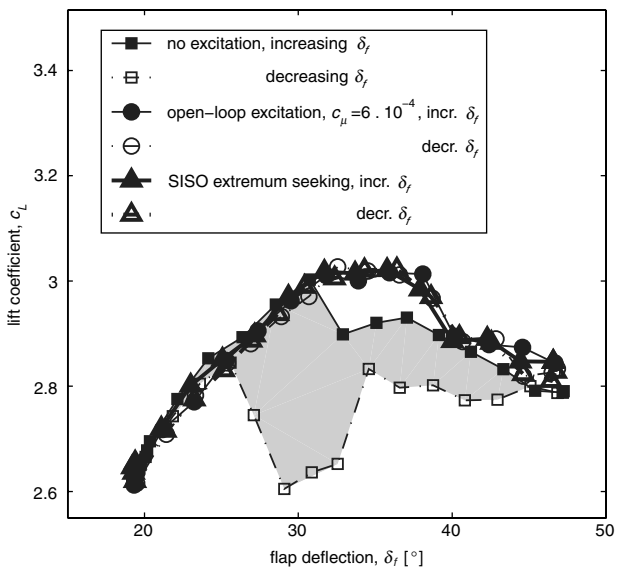


**Fig. 8 Lift coefficient $c_L$ vs flap deflection angle $\delta_f$ for increasing and decreasing $\delta_f$ without excitation, with permanent open-loop excitation ($c_\mu = 6 \times 10^{-4}$, constant pulse amplitude), and with closed-loop SISO extremum-seeking control ($Re_c = 0.5 \times 10^6$, $\alpha = 7$ deg).**

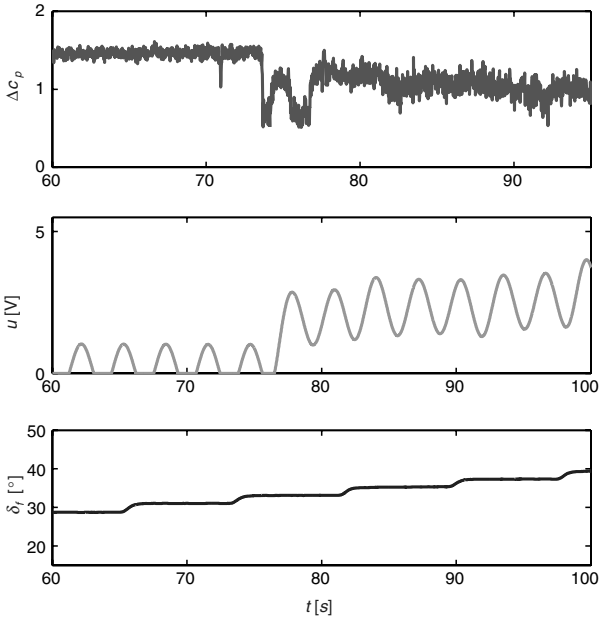


**Fig. 9 Time plot of closed-loop SISO extremum-seeking control experiment with varying flap deflection angle $\delta_f$ (cutout of Fig. 10b; $Re_c = 0.5 \times 10^6$, $\alpha = 7$ deg).**

SISO extremum-seeking control experiment with the nonexcited case and with the open-loop case with permanent excitation (constant amplitude of air pulses) is given in Fig. 8. Only data around the region with maximum lift are plotted. The lift increases as the flap is moved downwards. Without excitation, the separation occurs at $\delta_f \approx 31$ deg. By decreasing the angle $\delta_f$, a large hysteresis is visible, and is marked as the gray area in the figure. Reattachment of the flow does not occur until $\delta_f \approx 25$ deg. Both open- and closed-loop control delay flow separation by approximately 6 deg. The flow separates for higher $\delta_f$, but if $\delta_f$ is decreased afterwards, the hysteresis effect, which was noticed in the nonexcited case, vanishes almost completely. Because only a small gain in maximum lift is noticeable compared to the nonexcited case, the main advantage of this control is the delay of flow separation and the suppression of hysteresis. In this polar diagram no differences are discernible between the open- and closed-loop cases. However, closed-loop control offers benefits such as reduced power input, disturbance rejection, and robustness.

Figure 9 illustrates the dynamic behavior of the closed-loop extremum-seeking control in terms of pressure difference to be maximized and control input $u$, that is, the amplitude of the pulsed excitation, for increasing flap defection angle $\delta_f$. Notice that $u$ is superimposed with the sinusoidal perturbation $a \sin \omega t$ for gradient-based maximization. The high values of the pressure coefficient difference $\Delta c_p$ indicate that there is attached flow at low flap deflections, $\delta_f < 32$ deg at $t < 73$ s. The sinusoidal input perturbation of $u$ is distorted in this case, because negative amplitudes of excitation pulses are impossible from a physical point of view. Separation occurs at $t \approx 73$ s after a further stepwise increase of $\delta_f$, and there is also an abrupt pressure difference drop at this time instant. Now, the separated flow is sensitive to the sinusoidal input perturbation of $u$, resulting in an approximately sinusoidal perturbation of $\Delta c_p$ for $73 \leq t \leq 77$ s. Because the input and output perturbations are in phase, $\Delta c_p$ can be maximized by increasing the input $u$; this action is subsequently performed by the controller and leads to an increase of $\Delta c_p$. The maximization converges after about 1.5 perturbation periods; see the output signal in the time interval $73 < t < 77$ s. Again, the output perturbation vanishes when the flow reattaches.

Figure 10 shows the complete time series from which the open- and closed-loop flap polar diagrams in Fig. 8 are extracted. Both controls maximize the output $\Delta c_p$, which corresponds to maximum lift as observed in Fig. 8. Moreover, in Fig. 10 the advantage of closed-loop control is seen. Namely, the actuation $u$ is increased only when separation occurs. It can also be concluded from the magnitudes that less pressurized air is needed in the closed-loop case.

The disadvantage of this kind of extremum-seeking control is, however, that this scheme does not automatically decrease actuation after a changed flow condition would justify a lower $u$. For $\delta_f > 37$ deg ($98 < t < 178$ s), see the right side of Fig. 10, the continued excitation, whether in open- or closed-loop, is not able to reattach the flow. Hence, the actuation can be switched off, but this is not done by the closed-loop controller. Moreover, for $\delta_f < 25$ deg ($t > 226$ s), the flow reattaches without actuation. Again, the closed-loop

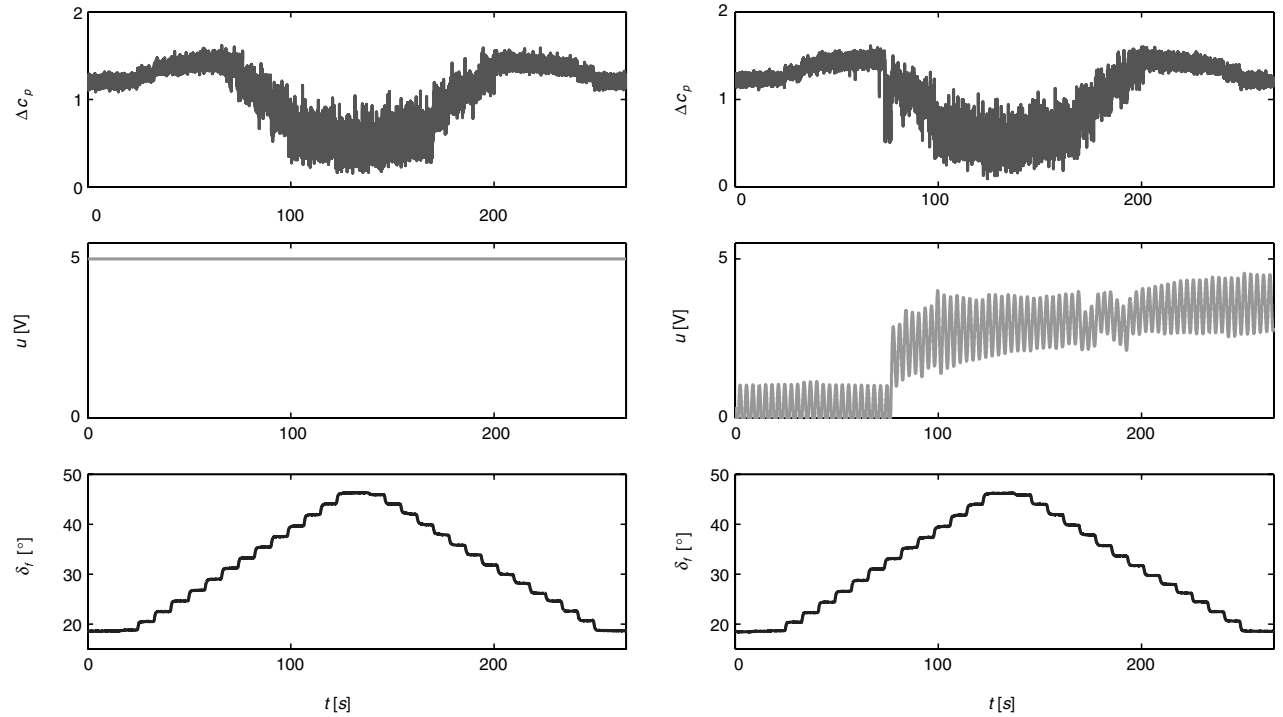


**a) Open-loop control with permanent actuation**

**b) Closed-loop SISO extremum seeking control (maximum seeking)**

**Fig. 10 Comparison of open- and closed-loop control for varying flap deflection angle $\delta_f$ ($Re_c = 0.5 \times 10^6$, $\alpha = 7$ deg).**

controller does not consider this scenario. This problem arises because the maximum $\Delta c_p$ is plateaulike and not a localized point. If the minimum necessary control input that maximizes $\Delta c_p$ decreases due to a change in flow condition, the extremum-seeking control is unable to detect the gradient. Hence, it cannot react to those changes.

### C. Extension to SISO Slope Seeking

The problem of the extremum-seeking scheme described in the preceding section can be solved by using a slope-seeking controller. In contrast to the steady-state input–output map in the sketch in Fig. 5, see the right side, the maximum of the high-lift system output is not characterized by a clear local extremum, $y^* = f(u^*)$, obtained for a certain value $u^*$ of the control input. Instead, the sketch in Fig. 6, see the right side, with a plateau gives a better indication of the required input–output map. In fact, the flow completely attaches, that is, the output is maximized, if the control input exceeds a certain threshold depending on the varying flow conditions. A further increase in $u$ does not lower $\Delta c_p$, as assumed in Fig. 5, but the flow remains attached. In such a case, with no clearly defined maximum, the controller does not decrease its output $\hat{u}$ or $u$, when external changes, for example, flow conditions, would justify a lower actuation. To avoid the controller from adjusting to too-high output values, $u > u^*$, thereby driving the system into saturation, the extremum-seeking control is extended by slope seeking [26]. The idea is to find the crossover from the separated to the attached flow state, that is, given by a small positive slope $\partial f(u)/\partial u$ of the steady-state input–output map, $y = f(u)$. By this approach, the minimum necessary control output is adjusted. Therefore, the negative value of the commanded slope, $f'_{\text{ref}}$, that is, a tuning parameter of the controller design, is also added to the detected slope; see Fig. 6.

Figure 11a shows the force balance measurement results of a SISO slope-seeking control experiment in comparison to the open-loop case with permanent excitation. The change of the crossover from the separated to the attached flow due to the closed-loop control, results in a slightly lower lift for high flap deflection angles $\delta_f$. This small difference, however, does not seem to be significant from a practical standpoint.

Again, the corresponding time series of the output signal $\Delta c_p$ and the control input $u$ adjusted by slope seeking during the variation of the flap deflection are displayed on the right side of this figure. The slope-seeking controller reduces the excitation such that the mimimum necessary control input $u$ is given to the actuator at all flow conditions. This is most clearly seen at $t \approx 100$ s, where the controller decreases the input signal $u$, because the excitation is not able to reattach the flow. When flap angles are smaller, the excitation increases again at $t \approx 180$ s ($\delta_f = 37$ deg) to reattach the flow. At $t \approx 207$ s, which corresponds to $\delta_f = 25$ deg, the control part $\hat{u}$ is switched off again (except the sinusoidal perturbation $a \sin \omega t$), because the flow remains attached.

### D. Extension to MIMO Slope-Seeking Design

#### 1. *MIMO Slope Seeking Setup*

To account for the flow separation that is not constant across the span of the flap, the measured pressure differences and the actuation are divided into three spanwise segments. Each segment provides one averaged output to be controlled, that is, a spanwise-averaged pressure difference over the segment span that is determined from one control input that gives uniform excitation over the segment span. Figure 12 shows this setup. The control segment to the right includes four actuator segments and the average pressure difference of four associated pressure transducers. The middle section contains three actuator–sensor pairs, whereas the left side again includes four actuator–sensor pairs.

The spanwise extent of the actuation was a compromise between system complexity and the spanwise influence of each actuator. On the one hand, each actuator has a limited spanwise influence, therefore the actuation may be selected to be small enough to account for the relevant spanwise dimension of local separation regions. On the other hand, the pressure difference output from each segment is affected by each control input and a small spanwise extent of the segment results in complex cross-coupling effects that must be considered in the controller design. In this investigation, the segments are sufficiently large that there is negligible coupling between the pressure differences of each segment and the adjacent

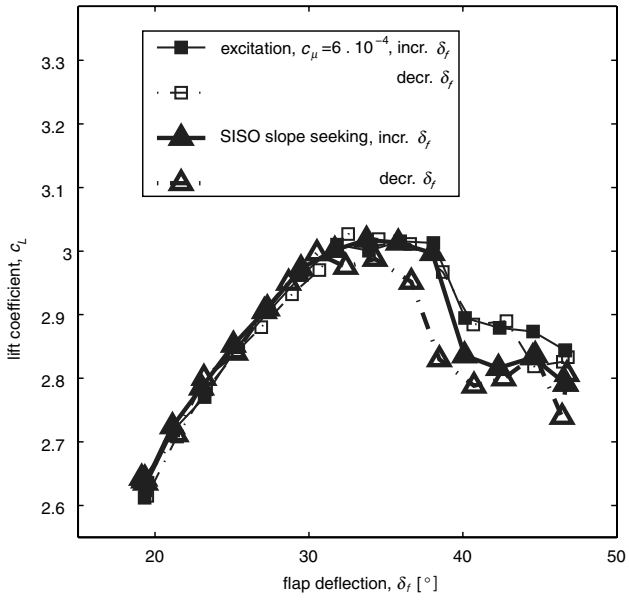


**a) Lift coefficient $c_L$ versus flap deflection angle $\delta_f$ for increasing and decreasing $\delta_f$ with permanent openloop excitation ($c_\mu$= 6·10$^{-4}$, constant pulse amplitude), and with closed-loop control**

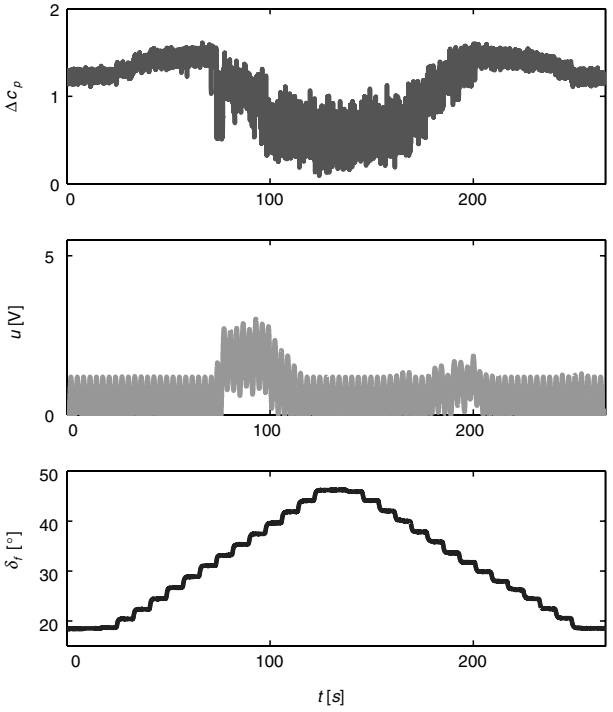


**b) Time plot of SISO closed-loop control experiment.**

**Fig. 11 Effect of closed-loop SISO slope-seeking control for varying flap deflection angle $\delta_f$ ($Re_c = 0.5 \times 10^6$, $\alpha = 7$ deg).**

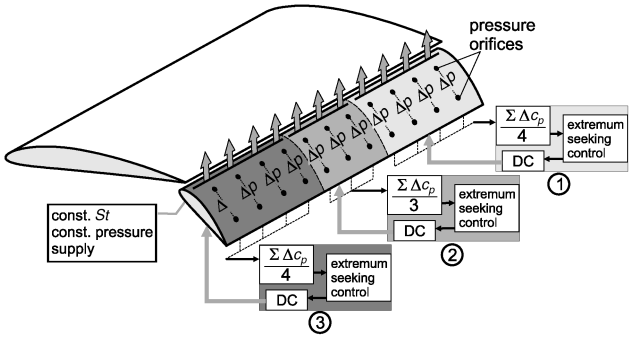


**Fig. 12 Sketch of the spanwise MIMO control setup with duty cycle as distributed control signal and pressure difference as spanwise distributed output signal to be controlled (DC: duty cycle of solenoid valves).**

control inputs. In the end, however, the number of individual segments was determined by the computing power available in the controller used. Hence, three decoupled (individual) extremum-seeking controllers, that is, three SISO controllers are used to maximize the pressure difference of each segment.

Although the spanwise cross coupling between the control segment inputs and the neighboring pressure difference responses is very small, the extremum-seeking control signal processing is made insensitive to any unintended cross-coupling effects. A phase shift of $\Delta\varphi = \pi/2$ between neighboring perturbations is introduced, following Ariyur and Krstic [26]. Thus, the harmonic input perturbation $a\cos\omega t$ and the demodulation signal $\cos\omega t$ are applied to the middle segment, whereas in the left and right segments we use $a\sin\omega t$ and $a\sin\omega t$, respectively.

Because the system has multiple inputs and multiple outputs and some cross coupling does exist, we still refer to a MIMO control setup despite the use of uncoupled controllers.

The design of the actuator in the present work does not provide for the individual control of the excitation amplitudes along the span. This is due to the fact that the 11 actuator segments share a common pressure supply, which is controlled by one pressure regulator valve. More valves could not be installed due to the limited size of the model. The duty cycle (set as 0.5 in open-loop cases, that is, the valves are open half of the period and otherwise closed) and frequency are the two actuator parameters, which can provide individual control of each spanwise segment. In the present work, the duty cycle of each segment is chosen as control input $u$, because individual valves may be closed ($u = 0$), whereas other segments have a pulsating jet ($0 \le u \le 0.5$). The forcing frequency is determined in preliminary tests and reflects only a compromise. Delaying separation and reattaching an already separated flow need different forcing frequencies [28,29]. Because the actuator does not allow for very high excitation frequencies in the order of $St = 3$ or even higher, the frequency for the closed-loop tests is set to a Strouhal number close to 1 that works well for flow reattachment and reasonably well for separation delay. To use an optimal excitation, the frequency has to be adjusted to every flap deflection because there is a slight dependency. This is not accounted for in these experiments.

The excitation amplitude is controlled by the supply pressure, which is set to a fixed value as well. In the open-loop case a prior performed calibration in still air yields the nondimensional blowing momentum coefficient. Because the controller constantly adjusts the duty cycle, a $c_\mu$ for the closed-loop results cannot be given.

### 2. *Results*

The results are presented in Fig. 13a in terms of lift for varying flap deflection. The angle of attack is fixed at $\alpha = 7$ deg. The line marked with square symbols represents the open-loop case with maximum forcing (duty cycle $u = 0.5$) as shown previously in Figs. 8 and 11a. The second pair of lines in the figure (triangle symbols) shows the lift in MIMO closed-loop control mode. The closed-loop controller increases the lift by an additional 2% over the open-loop control due to the adaption of the duty cycle. Even for smaller deflection angles $\delta_f < 30$ deg, where the flow is attached, a slight increase in lift can be observed in the closed-loop case. It is speculated that the spanwise varying actuation may produce 3-D structures, which suppress the

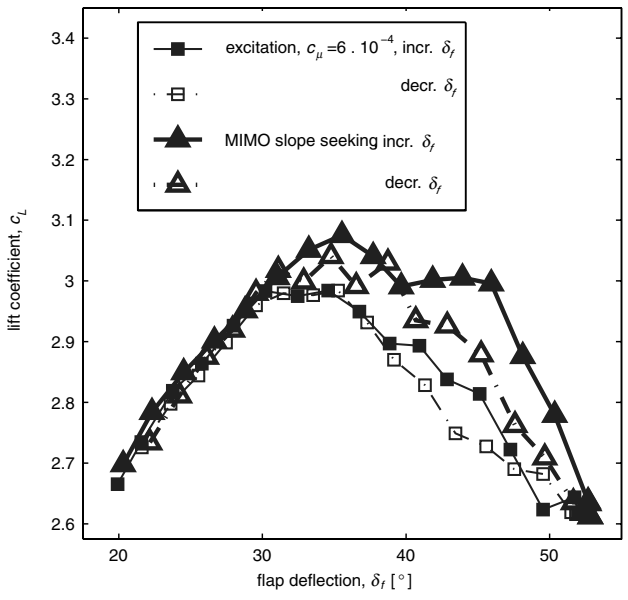


**a) Lift coefficient $c_L$ versus flap deflection angle $\delta_f$ for increasing and decreasing $\delta_f$ with permanent open-loop excitation ($c_\mu = 6{\cdot}10^{-4}$, constant pulse amplitude and duty cycle $u = 0.5$), and with closed-loop control**

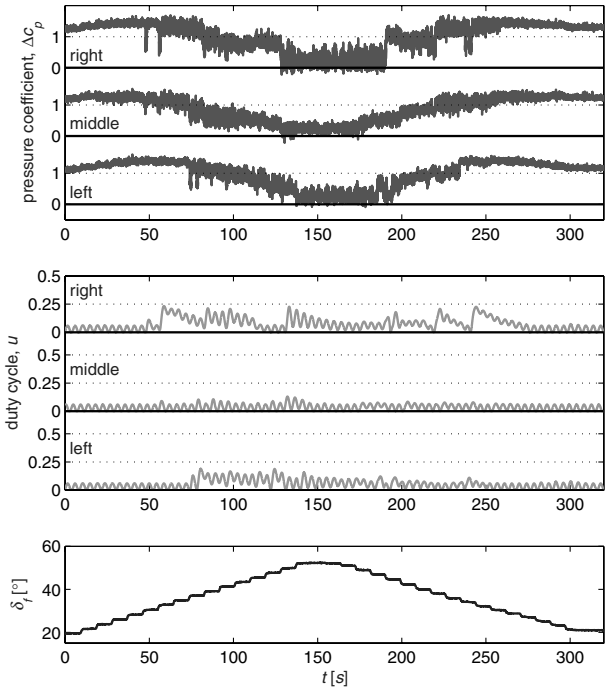


**b) Time plot of MIMO closed-loop experiment**

**Fig. 13 Effect of closed-loop MIMO slope-seeking control ($Re_c = 0.5 \times 10^6$, $\alpha = 7$ deg).**

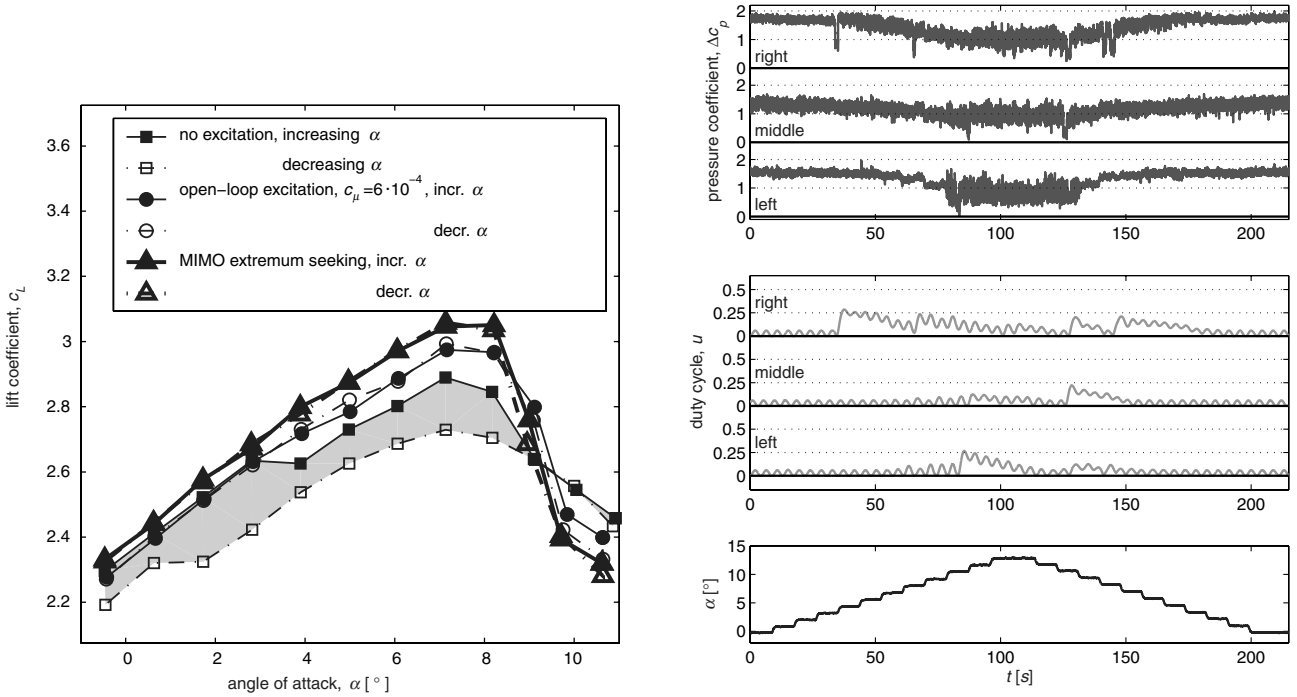


**a) Lift coefficient $c_L$ versus angle of attack $\alpha$ for increasing and decreasing $\alpha$ without excitaion, with permanent open-loop excitation ($c_\mu = 6{\cdot}10^{-4}$, constant pulse amplitude and duty cycle $u = 0.5$), and with closed-loop control**

**b) Time plot of MIMO closed-loop experiment**

**Fig. 14 Closed-loop MIMO slope-seeking control for varying angle of attack $\alpha$ ($Re_c = 0.5 \times 10^6$, $\delta_f = 33$ deg).**

short-time separations more effectively. It should be noted, however, that the comparison is based on open-loop experiments, in which only a duty cycle of 0.5 is used.

Figure 13b shows the time series of the pressure differences to be controlled, the control input for each of the three control segments, and $\delta_f$, from which the corresponding polar diagram is extracted for the MIMO control experiment. The very different spanwise control behaviors are noticed. The control segment to the right detects a separation event at $t = 48$ s ($\alpha = 30$ deg) and thus increases the duty cycle to $u = 0.23$, which is about half of the maximum. Despite the 2-D setup, the segment to the left detects a flow separation at $t = 74$ s ($\alpha = 37$ deg) and therefore increases $u$. The control signal of the midsection does not vary significantly until larger angles of attack are reached. Thus, the side walls are thought to enhance the flow separation on the left and right segments and as can be seen form the pressure differences the actuation on the outer segments has an influence on the middle section.

Once the control input $u$ is increased, see, for example, the time series $u(t)$ of the right segment in Fig. 13b, the controller slowly decreases $u$. This is a result of the slope-seeking extension to find the smallest necessary $u$. The controller seeks the crossover from separated to the attached flow that is given by a small positive slope in the system input–output characteristic. This seeking area is the result of the hysteresis behavior.

These results clearly show that spanwise MIMO controllers are required for separation control in real environments where there is spanwise variation in the separation. The MIMO slope-seeking control improves the performance of separation flow management compared to the SISO case that is described in Sec. IV.C. To further validate this self-adapting control, additional experiments that include changes of the flap deflection angle $\delta_f$ and variations in the angle of attack $\alpha$ and the Reynolds number $Re_c$ are considered.

Figure 14a shows force balance measurements for $\alpha$ variation for flow without excitation, open-loop, and MIMO closed-loop control. The flap deflection angle is fixed to $\delta_f = 33$ deg. Periodic excitation in the open-loop case (circled symbols) suppresses flow separation on the flap, which results in a delay of separation by about 5 deg and an increase in maximum lift of about 3% compared to the unexcited case (square symbols). These results are comparable to those obtained when the flap deflection is varied; see Fig. 13. The third pair of lines in this figure (triangle symbols) shows the corresponding results of the MIMO closed-loop mode. The controller provides a further increase in the lift of approximately 3% due to adaption in the duty cycle. It is surprising that the whole polar of the MIMO closed-loop case is shifted towards higher lift values compared to the other two cases.

There are two possible explanations for this behavior. First of all, in this 2-D setup there are secondary separation regions due to the sidewalls on the main wing and on the flap. There is a chance that in some way the MIMO control influences these secondary separation regions, and lift is increased due to their elimination, but flow visualizations did not confirm this behavior. Nineteen percent of the flap span is not covered by an excitation slot, of which 8% (100 mm) is located on each side of the flap close to the sidewalls due to the flap deflection angle adjustment mechanism. Hence, these secondary flow separation regions are not directly affected by the excitation. The other reason why MIMO control shows better results than the open-loop case could be due to local flow separations around the flap tracks. There are four flap tracks along the span where the flap is mounted to the main wing. In the vicinity of these mounting points, the excitation slot is interrupted. During flow visualization tests it has been observed that the flow separates in these regions early and excitation in a 2-D mode (open loop) is sometimes not able to fully reattach the flow behind the flap mounting. In this case the open-loop results do not represent the maximum lift gain possible. The improved lift even at very low angles of attack may come from an improved flow in the vicinity of the flap mounting points due to the 3-D excitation of the closed-loop setup.

The closed-loop results presented here are compared to the best results achieved for open-loop control, which were obtained by trial and error. There had been many attempts to improve the open-loop control by tuning the excitation parameters manually, including the duty cycle and using 3-D modes (spanwise varying excitation) instead of 2-D modes. However, the closed-loop performance was not obtained, which yielded only marginal improvements. There is still a chance that the closed-loop results can be achieved with a good

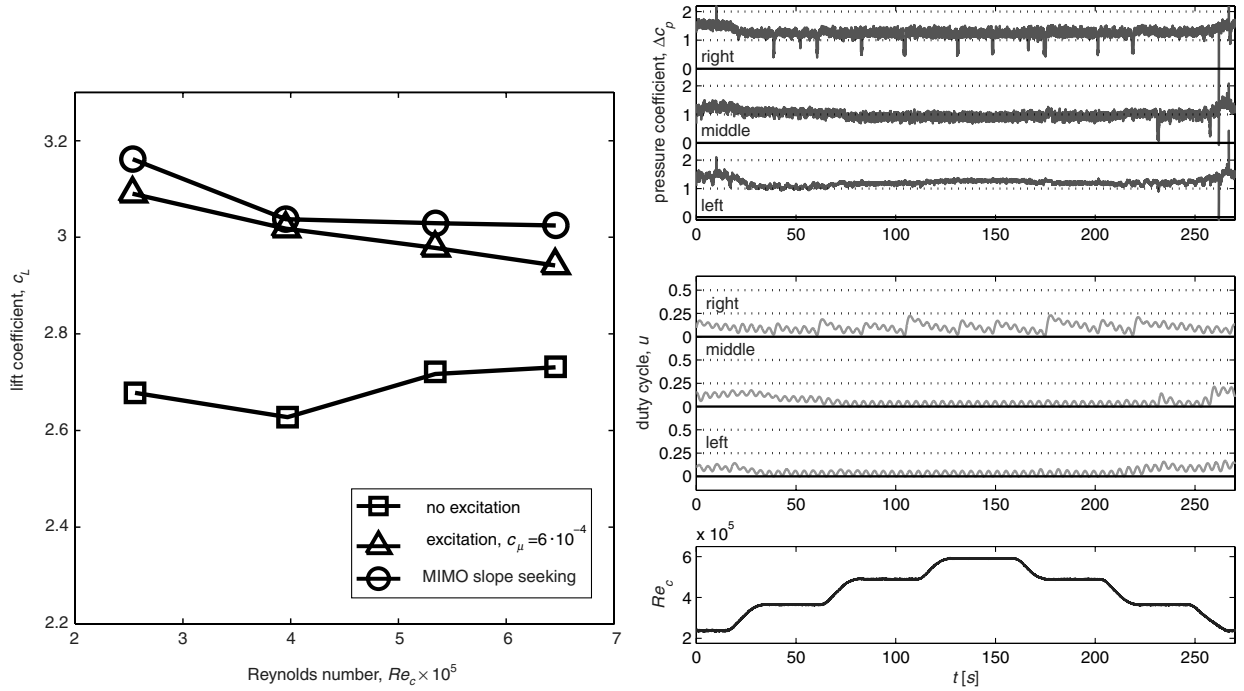


**a) Lift coefficient $c_L$ versus Reynolds number $Re_c$ without excitation, with permanent open-loop excitaion ($c_\mu = 6 \cdot 10^{-4}$, constant pulse amplitude and duty cycle $u = 0.5$), and with closed-loop control**

**b) Time plot of MIMO closed-loop experiment**

**Fig. 15 Closed-loop MIMO slope-seeking control for varying Reynolds number $Re_c$ ($\alpha = 7$ deg, $\delta_f = 35$ deg).**

set of manually adjusted excitation parameters in open loop as well, but it may take a long time to find these parameters. In our case, closing the loop found these parameters within seconds. This is another advantage of closed-loop experiments.

The corresponding time plots of the aforementioned closed-loop signals are shown in Fig. 14b. Again, the very different control behavior of the three segments is noticed. Around $\alpha = 2$–3 deg, when there is a decrease in the lift in the unexcited case is noticed, the control segment on the right detects a flow separation and the duty cycle is increased, reaching a value of 0.25 (that is, the solenoid valves are open for a fourth of the period). The other two control segments detect flow separations later and adjust their control inputs accordingly. Again, all control segments show the slowly decreasing control input due to the slope-seeking strategy and the hysteresis in the system. If the duty cycle is too small (after 65 s on the right segment), the flow separates for a very short time, see $\Delta c_p(t)$, and the control variable is immediately increased to regain lift. The control output of the midsection is not increased at all until larger angles of attack are reached.

To demonstrate the flexibility of MIMO slope seeking for arbitrary flow condition changes, Fig. 15 shows the results with different Reynolds number $Re_c$. Fig. 15a illustrates lift coefficient $c_L$ vs increasing $Re_c$ without excitation, with open-loop excitation, and with MIMO slope-seeking control. Here, open- and closed-loop excitation eliminate flow separation at low Reynolds numbers, $Re_c < 5 \times 10^5$, resulting in a significant lift increase. Again, real-time optimization by slope seeking increases the lift compared to open-loop control. The corresponding time plots of MIMO closed-loop control are displayed in Fig. 15b. The control segment on the right detects a separation at all Reynolds numbers and adjusts the excitation, accordingly.

## V. Conclusions

This paper describes a successful approach for closed-loop separation control by active means on a generic high-lift configuration, that is, a 2-D wing with a single-slotted trailing-edge flap. Well-known local periodic forcing near the leading edge of the flap is used to excite the flow to maximize the lift due to minimization or delay of flow separation. Because closed-loop flow control suffers from the lack of sufficient simple low-dimensional models for this configuration accessible for controller synthesis methods, here, a non-model-based real-time optimization scheme that guarantees closed-loop stability, namely, the well-known extremum-seeking control, is used for the adjustment of the control input.

Starting from the basic extremum-seeking control scheme, two advanced setups using a single-input/single-output and a multi-input/multi-output slope-seeking design are tested in wind-tunnel experiments. The effect of closed-loop control on the lift is monitored by force balance measurements. Closed-loop slope-seeking control turned out to be more efficient than open-loop control, because excitation is used only if a flow separation is detected. Furthermore, the controller is able to adjust the control input in a least necessary sense. This even includes the switching off of the actuation when the flow reattaches by itself due to flow condition changes or if excitation is noneffective, for example, during high angles of attack or high flap deflections. An advantage of this closed-loop scheme is that no controller design model is needed and that it accounts for varying flow conditions automatically, such that no gain scheduling is needed as common in flight control. A disadvantage is the very low bandwidth of the closed-loop system due to the requirements concerning the perturbation frequency $\omega$. Therefore, the closed loop should be extended by open-loop components or by combination with other control loops as done by Garwon and King [16] to account for fast disturbances. For these cases, extremum-seeking control provides a basic optimization that should be extended by fast control loops.

The results, however, clearly indicate that spanwise MIMO control is needed for 3-D, real flight configurations to account for spanwise distributed separation. MIMO slope-seeking control appears to be a good candidate for the successful, and robust flow management in many applications. Its flexibility concerning separation suppression during different flow condition changes is demonstrated in terms of variation of the angle of attack, flap deflection angle, and Reynolds number.

## Acknowledgment

This work was partially supported by the Deutsche Forschungsgemeinschaft (German Science Foundation) in the context of the Collaborative Research Centre (Sfb) 557 "Control of complex turbulent shear flows."

## References

[1] Fiedler, H., and Fernholz, H., "On the Management and Control of Turbulent Shear Flows," *Progress in Aerospace Sciences*, Vol. 27, No. 4, 1990, pp. 305–387.

[2] Gad-el-Hak, M., Pollard, A., and Bonnet, J.-P. (eds.), *Flow Control: Fundamentals and Practices*, Springer–Verlag, Berlin, 1998.

[3] Gad-el-Hak, M., and Bushnell, D., "Separation Control: Review," *Journal of Fluids Engineering*, Vol. 113, March 1991, pp. 5–29.

[4] McLean, J., Crouch, J., Stoner, R., Sakurai, S., Seidel, G., Feifel, W., and Rush, H., "Study of the Application of Separation Control by Unsteady Excitation to Civil Transport Aircraft," NASA Technical Report CR-1999-209338, 1999.

[5] Pack, L., Schaeffler, N., Yao, C.-S., and Seifert, A., "Active Control of Flow Separation from the Slat of a Supercritical Airfoil," AIAA Paper 2002-3156, 2002.

[6] Pack, L., Yao, C.-S., and Seifert, A., "Active Control of Separation from the Flap of a Supercritical Airfoil," *AIAA Journal*, Vol. 44, No. 1, 2006, pp. 33–41.

[7] King, R., Seibold, M., Lehmann, O., Noack, B., Morzynski, M., and Tadmor, G., "Nonlinear Flow Control Based on a Low Dimensional Model of Fluid Flow," *Lecture Notes in Control and Information Science*, Vol. 322, edited by T. Meurer, K. Graichen, and E. D. Giles, Springer–Verlag, Berlin, 2005, pp. 365–386.

[8] Caraballo, E., Yuan, X., Little, J., Debiasi, M., Yan, P., Serrani, A., Myatt, J., and Samimy, M., "Feedback Control of Cavity Flow Using Experimental Based Reduced Order Model," AIAA Paper 2005-5269, 2005.

[9] Glauser, M., Higuchi, H., Ausseur, J., and Pinier, J., "Feedback Control of Separated Flows," AIAA Paper 2004-2521, 2004.

[10] Siegel, S., Cohen, K., and McLaughlin, T., "Experimental Variable Gain Feedback Control of a Circular Cylinder Wake," AIAA Paper 2004-2611, 2004.

[11] Allan, B., Juang, J.-N., Raney, D., Seifert, A., Pack, L., and Brown, D., "Closed-Loop Separation Control Using Oscillatory Flow Excitation," NASA Technical Report CR-2000-210324, Institute for Computer Application in Science and Engineering (ICASE) Report No. 2000-32, 2000.

[12] King, R., Becker, R., Garwon, M., and Henning, L., "Robust and Adaptive Closed-Loop Control of Separated Shear Flows," AIAA Paper 2004-2519, 2004.

[13] Becker, R., Garwon, M., and King, R., "Development of Model-Based Sensors and Their Use for Closed-Loop Control of Separated Shear Flows," *Proceedings of the European Control Conference 2003*, Univ. of Cambridge, Cambridge, England, U.K., 2003.

[14] Becker, R., Garwon, M., Gutknecht, C., Bärwolff, G., and King, R., "Robust Control of Separated Shear Flows in Simulation and Experiment," *Journal of Process Control*, Vol. 15, No. 6, 2005, pp. 691–700.

[15] Becker, R., and King, R., "Comparison of a Robust and a Flatness Based Control for a Separated Shear Flow," *Proceedings of the 16th IFAC World Congress*, International Federation of Automatic Control, 2005.

[16] Garwon, M., and King, R., "A Multivariable Adaptive Control Strategy to Regulate the Separated Flow Behind a Backward-Facing Step," *Proceedings of the 16th IFAC World Congress*, International Federation of Automatic Control, 2005.

[17] Henning, L., and King, R., "Drag Reduction by Closed-Loop Control of a Separated Flow over a Bluff Body with a Blunt Trailing Edge," *Proceedings of the 44th IEEE Conference on Decision and Control and European Control Confernce, CDC-ECC'05*, IEEE, New York, 2005.

[18] Banaszuk, A., and Narayanan, S., "Adaptive Control of Flow Separation in a Planar Diffuser," AIAA Paper 2003-0617, 2003.

[19] Garwon, M., Urzynicok, F., Darmadi, L., King, R., and Bärwol, G., "Adaptive Control of Separated Flows," *Proceedings of the European Control Conference 2003*, Univ. of Cambridge, Cambridge, England, U.K., 2003.

[20] Beaudoin, J.-F., Cadot, O., Aider, J.-L., and Wesfried, J.-E., "Drag Reduction of a Bluff Body Using Adaptive Control Methods," *Physics of Fluids*, Vol. 18, No. 8, Aug. 2006, pp. 085107-1–085107-10.

[21] Petz, R., Nitsche, W., Becker, R., and King, R., "Lift, Drag and Moment Control on a High-Lift Configuration by Means of Active Flow Control," *Proceedings of the CEAS/KATnet Conference on Key Aerodynamic Technologies*, Deutsche Gesellschaft fuer Luft- und Raumfahrt (DGLR), Bremen, Germany, 2005.

[22] Petz, R., and Nitsche, W., "Active Separation Control on a High-Lift Configuration by a Periodically Pulsating Jet," *Proceedings of the 24th International Congress of the Aeronautical Sciences*, Optimage, Edinburgh, U.K., 2004.

[23] Barlow, J., Rae, W., and Pope, A., *Low Speed Wind Tunnel Testing*, 3rd ed., John Wiley & Sons, Amsterdam, 1990.

[24] Greenblatt, D., and Wygnanski, I., "The control of Flow Separation by Periodic Excitation," *Progress in Aerospace Sciences*, Vol. 36, No. 7, 2000, pp. 487–545.

[25] Wang, H.-H., Yeung, S., and Krstic, M., "Experimental Application of Extremum Seeking on an Axial Flow Compressor," *Proceedings of the American Control Conference 1998*, International Federation of Automatic Control, 1998.

[26] Ariyur, K., and Krstic, M., *Real-Time Optimization by Extremum-Seeking Control*, John Wiley & Sons, Hoboken, 2003.

[27] Krstic, M., and Wang, H.-H., "Stability of Extremum Seeking Feedback for General Nonlinear Dynamic Systems," *Automatica*, Vol. 36, No. 4, 2000, pp. 595–601.

[28] Darabi, A., and Wygnanski, I., "Active Management of Naturally Separated Flow over a Solid Surface. Part 1. The Forced Reattachment Process," *Journal of Fluid Mechanics*, Vol. 510, July 2004, pp. 105–129.

[29] Darabi, A., and Wygnanski, I., "Active Management of Naturally Separated Flow over a Solid Surface. Part 2. The Separation Process," *Journal of Fluid Mechanics*, Vol. 510, July 2004, pp. 131–144.

N. Chokani
*Associate Editor*